

Flow Stability Model of Centrifugal Compressors Based on Eigenvalue Approach

Xiaofeng Sun* and Yunfei Ma†

Beihang University, 100191 Beijing, People's Republic of China

Xiaohua Liu‡

Civil Aviation Administration of China, 100102 Beijing, People's Republic of China

and

Dakun Sun§

Beihang University, 100191 Beijing, People's Republic of China

DOI: 10.2514/1.J054350

A stall inception model of centrifugal compressors is developed on the basis of the global stability analysis in the present paper. This model takes specific flow patterns and impeller geometry into account, which can be used to analyze the effect of blade design parameters on the stall limit of centrifugal compressors. In particular, the body force model and the solution of the stability eigenvalue equation are two important problems to be addressed in this frame. The spectral method and singular value decomposition are used to discrete stability equations to obtain the eigenvalues. By applying conservation laws, a perturbation-response form of the body force, specifically for centrifugal compressor, is also established to simulate blade behavior. Two different forms (the meridional model and the normal expansion model) are derived to make a comparison of grid independence and computation time. The capacity of these models is assessed against the experimental data of a NASA low-speed centrifugal compressor rotor. The results show that these models could be used to predict stall onset with acceptable accuracy and low computational cost.

Nomenclature

$A, B, C, D, E, G,$	= coefficient matrices
H, P, Q, R, T	
c_v	= specific heat at constant volume
\mathbf{F}	= body force vector
F_d	= force density
$\mathbf{F}^N, \mathbf{F}^T$	= normal and tangential body force matrices
f	= blade force
i	= imaginary unit
k	= undetermined body force coefficient
m	= circumferential mode number
n	= normal to streamline coordinate in meridional plane
p	= fluid static pressure
R	= gas constant
r, θ, z	= cylindrical coordinates
t	= time
U, S, V	= column-orthogonal, diagonal, and orthogonal matrices
v	= fluid velocity vector
η, ξ	= rectangular coordinates in computational plane
μ	= loss coefficient
ρ	= fluid density
τ	= viscosity tensor

τ	= time-delay constant
Φ	= column vector of perturbation
Ω	= rotational speed of impeller, revolutions/s
ω	= eigenfrequency of the system
ω_r, ω_i	= real part and imaginary part of eigenfrequency

I. Introduction

CENTRIFUGAL compressors, as a part or a whole, are widely used in various areas such as chemical machinery, power stations, turbochargers assembled in numerous automobiles, and turboshaft engines installed in flight vehicles. Especially for aircraft engines, the centrifugal compressors must meet the high-pressure ratio requirements of the application in order to keep a compact engine size and light weight. Besides, the relevant design must also be aimed at high operation efficiency and low energy consumption throughout the entire operating envelope. To meet such requirements, the current trend has been toward highly loaded blade designs in order to increasingly advance the stage pressure ratio. It is known that a high-pressure rise design is prone to induce unsteady phenomena such as stall and surge, which may even result in catastrophic damage to the whole devices. This indeed poses a major design challenge for highly loaded centrifugal compressors with both advanced performance and a wide operation range. Therefore, how to judge and extend the operation range of the centrifugal compressors with high efficiency in the design phase have long been problems of importance.

Some remarkable attempts have enhanced the operation range through various modern methods such as the active control technique [1], air injection [2], variable-inlet guide vanes [3], circumferential throttling [4], and tangential blowing [5]. These techniques indeed offered great potential for future possible applications. However, they still needed some further investigation before being put into practical use. In contrast, it was found that the combination design of a swept and skewed blade could have an obvious influence on the stability limit of centrifugal compressors. Especially, it was reported by Rodgers [3] that impeller designs with increased backsweep could yield an improved operation range. However, the relationship between the operation range and the sweep and skewing variation of the blade was not clear, which was mainly dependent on either experimental observation or the steady flow analysis with empirical

Received 15 March 2015; revision received 29 September 2015; accepted for publication 19 November 2015; published online 13 June 2016. Copyright © 2015 by the American Institute of Aeronautics and Astronautics, Inc. All rights reserved. Copies of this paper may be made for personal and internal use, on condition that the copier pay the per-copy fee to the Copyright Clearance Center (CCC). All requests for copying and permission to reprint should be submitted to CCC at www.copyright.com; employ the ISSN 0001-1452 (print) or 1533-385X (online) to initiate your request.

*Professor, School of Power and Energy Engineering; sunxf@buaa.edu.cn.

†Ph.D. Candidate, School of Power and Energy Engineering; mayunfei@buaa.edu.cn.

‡Engine Certification Center; liuxh@buaa.edu.cn.

§Assistant Professor, School of Power and Energy Engineering; sundk@buaa.edu.cn (Corresponding Author).

data. But, the operation range or stall margin, after all, was a flow stability problem. There was reason to believe that the stability model should play a more important role in judging the stability limit. On the other hand, some flow stability models were available for centrifugal compressors [3,6–8]. These models revealed some complex mechanisms associated with the generation and development of rotating stall. However, due to oversimplified assumptions for flow and blade geometry, as well as the requirement of experimental results as input, these models might not have been suitable for analyzing the effect of the backsweep blade design on the operation range. Therefore, a stability model was imminently needed to judge the stability limit without sacrificing the complex flow and geometry of the blade.

Two ways may achieve this objective. The first is to directly solve unsteady Reynolds-averaged Navier–Stokes (URANS) equations as a kind of initial boundary value problem to obtain the relating flowfield information from the stall precursor to fully developed rotating stall. Over the past decades, numerical simulations based on URANS and high-order spatial discretization schemes have established themselves as a widely used tool to study complex flow problems in turbomachinery. They aim at capturing all relevant physical features of the flow by spatially resolving all dynamic scales, such as the modal waves and spikes discovered in such numerical models [9]. The range of applications of state-of-the-art URANS-based approaches in turbomachinery is truly impressive in scope and complexity. In 2000, Stein et al. [10] used an unsteady three-dimensional viscous flow solver to study flow stability in a high-speed centrifugal compressor and illustrated a growing process of reversed flow regions during the surge cycle in the meridional view. Recently, Chen et al. [11] proposed the time-accurate full-annulus three-dimensional Navier–Stokes code simulations of CC3 in parallel with the engine demonstrator test. They found very rich details of the development of stalling passages with reverse flow regions, which was also very helpful to understand the mechanism associated with the generation and development of the stall precursor. However, unsteady computational fluid dynamics (CFD) computation is time consuming, with up to several months, and highly dependent on where the initial perturbation is placed. Obviously, nowadays, it is difficult to apply such computational models as a design tool.

The alternative way is the eigenvalue method, which is widely used in various stability analyses. It is noted that linear hydrodynamic stability analysis plays a central role in identifying the dynamic behavior of infinitesimal perturbations superimposed on a steady-based flow. A classical tool to study the temporal instability of such flow is given by local stability theory, which in general relies on the existence of two homogeneous spatial coordinate directions and one inhomogeneous spatial coordinate direction. This approach dates back over nearly 100 years and leads to eigenvalue problems of moderate sizes, which can be solved by standard direct techniques. The calculation of eigenvalues is thus a crucial component for understanding the underlying mechanisms in a large variety of fluid-dynamical applications. The assumption of two homogeneous directions, however, restricts the local stability theory to flow with simple geometry and simple flow physics. More complex and technologically relevant flow situations with several inhomogeneous directions and/or complicated flow physics, such as supersonic flow around blunt bodies and complex flow around compressor blades, are beyond its reach. Instead, this type of flow situation requires a global rather than a local approach. In fact, it was due to such demands that the method of global stability analysis was born at the right moment. Now, this method has recently become the subject of intensive investigation [12,13], since Zebib [14] made a pioneering work in 1987. It has been applied to various flow stability problems such as flow separation [15], stall cells on airfoils [16], aircraft buffet boundaries [17], and acoustic resonance problems [18]. Lately, the global stability analysis has been extended to thermoacoustics problem; Li and Sun [19] developed a three-dimensional thermoacoustics instability model with emphasis on the effect of both axially and azimuthally inhomogeneous steady flows on the instability. This model provides us with a new scenario about how the vortex wave takes effect on the prediction of combustion instability.

For the flow stability in turbomachinery, besides requiring the consideration of the complex flow and geometry like global stability analysis, the most prominent difference between them is that the unsteady loading acting on the blade must be strictly included in any flow stability model of turbomachinery. The reason is that the flow instability mechanism in turbomachinery, to a large extent, originates from the unsteady fluctuation of the blade loading, which is completely different from the other flow stability problems, such as the flow transition mainly depending on the Reynolds number and velocity profile. In this regard, it is worth noting that Gordon [20] established an eigenvalue model for the analysis of an axial flow compressor along with the assumption of axisymmetric and incompressible Euler flows. Specifically, the rigorous treatment of the blade body force makes the eigenvalue model easy to solve, which is also attributed to the continuous contribution on the modeling of the blade body force from the Gas Turbine Laboratory [9,21] at the Massachusetts Institute of Technology. On the basis of global stability analysis, Sun et al. [22] developed a general eigenvalue approach to handle the three-dimensional instability problem in turbomachinery without simplifying the flow and geometry involved. In fact, Sirovich [23] proved that any immersed body in flow can be strictly replaced by a generalized function. This proof also constitutes the basis of the immersed boundary method widely used in moving flow boundary simulations [24]. Therefore, at the beginning of the theoretical model, it is not necessary to make any simplified assumption to the body force acting on the blades as many textbooks about turbomachinery did. Moreover, it is possible to obtain various reduced-order models for both the flow and body force in terms of different applications.

On the other hand, compared to the existing work for axial flow compressors, no work has established the stall inception model of centrifugal compressors based on global stability analysis. In principle, the existing models can be extended to be suitable for the stability analysis of centrifugal compressors. However, considering different flow patterns in centrifugal compressors and impeller geometry, some special difficulties related to the calculating method of eigenvalues and the model of the body force may be encountered. For the present investigation, there are thus two objectives. The first is to develop an appropriate computational method of eigenvalue specifically for the centrifugal compressor stability problem. It is noted that the eigenvalue solution methods used in current global flow stability analysis can be divided into two groups. The first one consists of algorithms destined for the small-dimensional problems. The representatives of this group are *QR*, *QZ* decomposition or Jacobi methods. The alternative methods are based on calculation of the invariant subspaces having dimensions significantly smaller than the original problem. In this paper, the relevant eigenvalue calculation will be presented on the basis of the aforementioned basic ideas and singular value decomposition (SVD), along with the application of spectral method. The other objective is to develop a body force model suitable for centrifugal compressor blades. Especially, the main focus will be placed on how the blade responds to any possible fluctuations. Thus, the fluctuating part of the body force must satisfy the physical requirements in any given environment.

With reference to the context, a stability model based on an eigenvalue approach for a centrifugal compressor is established in the present investigation. More important, besides giving a clear stability criterion, it also provides more insights into the mechanism of rotating stall inception. In particular, with the proposed theoretical frame, two specific models (called the normal expansion model and meridional model) are developed to investigate the most unstable mode as the stability criterion of centrifugal compressors. The assessment is also performed on a low-speed centrifugal compressor to compare the accuracy, computation time, and grid point independence of these two models.

II. Stall Inception Models for Centrifugal Compressor

A general centrifugal compressor impeller is illustrated in the meridional plane (see Fig. 1), which consists of inlet, blade, and outlet regions. The flowfield can be described by a group of three-

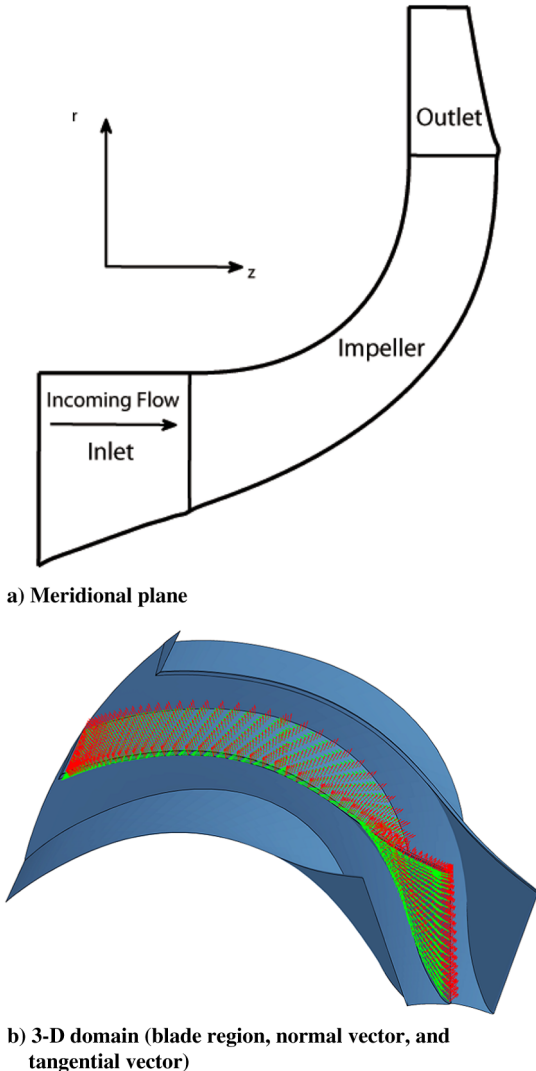


Fig. 1 Flow passage of the LSCC.

dimensional (3-D) unsteady, compressible Navier–Stokes (N-S) equations in a fixed frame of a cylinder coordinate system, in which the force terms represents the effect of the blade on fluid particle:

$$\begin{cases} \frac{\partial \rho}{\partial t} + \nabla \cdot (\rho \mathbf{v}) = 0 \\ \rho \frac{D\mathbf{v}}{Dt} = -\nabla p + \rho \mathbf{F} + \nabla \cdot \boldsymbol{\tau} \\ \frac{Dp}{Dt} + c_v p \nabla \cdot \mathbf{v} = (c_v - 1)(-\nabla \cdot \mathbf{q} + \boldsymbol{\tau} : \nabla \mathbf{v}) \end{cases} \quad (1)$$

where

$$\frac{D}{Dt} = \frac{\partial}{\partial t} + \mathbf{v} \cdot \nabla, \quad \nabla \cdot \boldsymbol{\tau} = \mu \Delta \mathbf{v} + \frac{1}{3} \mu \nabla (\nabla \cdot \mathbf{v})$$

For the flow instability phenomenon associated with centrifugal compressors, Lawless and Fleeter [25] observed the transition to stall in a low-speed centrifugal compressor was a gradual process, with the growth of the pressure waves that then dissipated as a stronger mode and gain dominance over the flowfield. In 2009, Spakovszky and Roduner [26] observed short wavelength disturbances, or so-called spikes in the vaneless space between the impeller and the vane diffuser. Whether modal waves or spike waves appear in turbomachinery, both of them could be expressed as a Fourier series. During the linear period of stall inception, perturbations are so small that the flow quantities can be assumed to consist of quantities averaged by time and small disturbances:

$$\Phi = \tilde{\Phi}(r, \theta, z) + \Phi'(r, \theta, z, t) \quad (2)$$

where $\Phi = [\rho, p, v_r, v_\theta, v_z]^T$; and the variables are nondimensionalized, respectively, by the reference pressure $\rho_0 U_0^2$, inlet velocity U_0 , and gas density ρ_0 before the inlet and reference length R_2 (radius of casing). By using the Fourier series, Φ' can be expanded as

$$\Phi' = \tilde{\Phi}(r, \theta, z) e^{-i\omega t} \quad (3)$$

Substituting this linear form into Eq. (1) obtains the matrix equation

$$\left(A \frac{\partial}{\partial r} + B \frac{\partial}{\partial \theta} + C \frac{\partial}{\partial z} + E \frac{\partial^2}{\partial r^2} + G \frac{\partial^2}{\partial z^2} + H \frac{\partial^2}{\partial r^2 \partial \theta^2} + P \frac{\partial^2}{\partial r \partial z} \right. \\ \left. + Q \frac{\partial^2}{\partial r \partial \theta} + R \frac{\partial^2}{\partial \theta \partial z} + D - i\omega T \right) \tilde{\Phi} = \mathbf{F} \quad (4)$$

where the coefficient matrices contain the basic quantities of steady flow calculated by a 3-D Reynolds-averaged Navier–Stokes (RANS) equations solver.

A. Body Force Model for Centrifugal Compressor

Many researchers have regarded the surface of blades as a boundary of the flow region; under this standpoint, the mathematical equation can be solved as an initial boundary value problem. However, for practical use, especially for unsteady flow, two essential disadvantages may occur:

1) Calculation of 3-D unsteady flow costs tremendous time and resources, especially for the intricate flow region.

2) The intensity and location of the perturbations introduced in the flowfield depend on the researcher's personal experience.

To tackle the problems in simulating the intricate boundary, Peskin [24] used a force term on the right-hand side of the momentum equation and obtained

$$\int \left(\rho \frac{D\mathbf{v}}{Dt} + \nabla p - \mu \Delta \mathbf{v} \right) dV = \mathbf{f} \quad (5)$$

where \mathbf{f} is the blade force acting on the flow region V . He introduced \mathbf{F}_d as the force density generated by the elasticity of the material and, by applying the theory of functional analysis, he finally demonstrated that

$$\mathbf{f}(\mathbf{x}, t) = \int \mathbf{F}_d(\mathbf{x}_0, t) \delta(\mathbf{x} - \mathbf{X}(\mathbf{x}_0, t)) d\mathbf{x}_0 \quad (6)$$

where δ is the Dirac delta function, and $\mathbf{X}(\mathbf{x}_0, t)$ is the configuration of the material, meaning the force only existed in the flow region close to the blade. Similarly, the blade here could also be regarded as an elastic material, the boundary of which could be replaced with force term (6). To simplify the problem, we assume that the force acts on every fluid particle in the blade region, so \mathbf{F}_d is distributed over the whole region, which leads to equation

$$\mathbf{f}(\mathbf{x}, t) = \int \mathbf{F}_d(\mathbf{x}, t) dV = \int \rho \mathbf{F}(\mathbf{x}, t) dV \quad (7)$$

where $\mathbf{F}(\mathbf{x}, t)$ is the mass force.

Generally, a force consists of three essential terms: magnitude, direction, and point of action. Actually, Peskin's immersed boundary method [24] has mathematically solved the third term, which transforms a concentrated force into a distributed force by using a continuous function to approach $\delta(\mathbf{x})$. For the sake of simplicity, $\delta(\mathbf{x})$ usually has many different forms like the Gauss function $f(x) = ae^{-(x-b)^2/c^2}$ and the generalized expansion of discontinuous functions [27–29], which is used in the immersed interface method for improving numerical accuracy.

First, from the forces and effects point of view, Marble [30] averaged the blade force on every fluid particle and gave a detailed scheme to simulate the effect of the blade force on the flowfield, and

he obtained simple formulas for force components. Goldstein et al. [31] modeled a nonslip flow boundary by using a novel technique to introduce solid surfaces into a simulated flowfield. Throughout the last two decades, a variety of body force models have been applied to represent the blades. Longley [32] deemed that the simulation of the blade passage body force not only drove the momentum changes of the flow but also specified the generation of the excess kinetic energy. As a result, he used the steady-state estimates of viscous losses and flow turning to simulate the effects of nonsteady flow. Based on the formulation developed by Marble [30], Chima [33] specified the blade passages in detail by using the body force term with accurate geometric relations and directions of motion. In 1999, conservation laws were separately applied in Gong et al.'s [34] and Gordon's [20] body force models for axial compressors. The former developed their model using a steady momentum equation to establish the relation between total pressure and body force components on the streamline, whereas the latter added a transform relation between the work of resistance and the loss of rotating total pressure.

Second, to orient the force, according to their works [20,33,34], it could be concluded that a blade force could be decomposed into two parts, a normal one and a tangential one (which is also a resistance), due to their effects as follows:

$$\mathbf{F} = \mathbf{F}_n + \mathbf{F}_t, \quad (8)$$

where the first term changes the direction of velocity, and the second term diminishes the magnitude of velocity. Unit vectors are illustrated in Fig. 2, where the vectors are shown for normal, tangential, and flowing directions. Figure 3 shows these vectors in the $z - \theta$ plane.

The last term we concerned about is magnitude of the body force, which can be further modeled by applying conservation laws due to its turning effect and dissipative effect acting on the flow. In the present work, a novel body force model is established for a centrifugal compressor, where the flow turns greatly in the axial, radial, and circumferential directions under the actions of the hub, shroud, and blades. Here, it is assumed that, in the circumferential direction of the moving coordinates, the force component is proportional to the radial velocity and the difference between the actual velocity $v_\theta - \Omega r$ and the theoretical velocity $v_{\text{rel}}\tau_\theta$ (v_{rel} is total relative velocity, and τ_θ is the circumferential component of unit vector in the ideal flow direction arranged by blade):

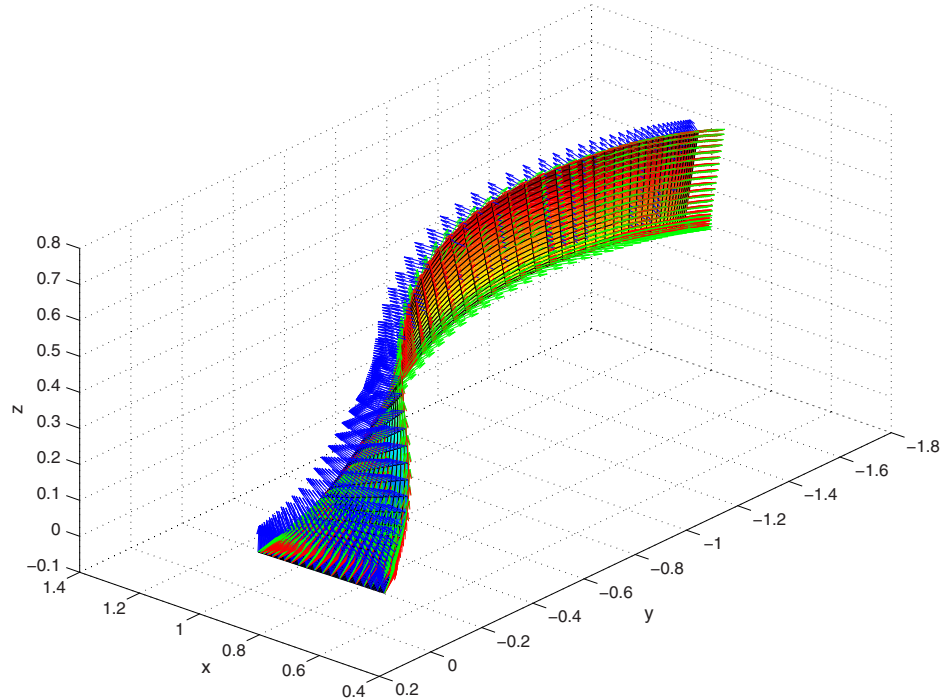


Fig. 2 Unit vectors of normal, tangential, and flowing directions in 3-D coordinates.

$$F_{n\theta} = kv_r[v_{\text{rel}}\tau_\theta - (v_\theta - \Omega r)] \quad (9)$$

Then, k can be obtained by the circumferential momentum equation

$$k = \frac{(\partial v_\theta / \partial r) + (v_x / v_r)(\partial v_\theta / \partial x) + (v_\theta / r)}{v_{\text{rel}}\tau_\theta - (v_\theta - \Omega r)} \quad (10)$$

On the other hand, the resistant force, on the basis of Hill and Peterson's work [35], is deemed to be proportional to the square of the total relative velocity, which gives

$$F_t = \mu v_{\text{rel}}^2 \quad (11)$$

According to Gordon's work [20], in rotating flow, the total pressure loss is measured by its change in rotary total pressure, expressed by $\bar{P}_t = P_t - \rho r \omega v_\theta$. By applying the relation between work and energy, we obtain

$$\Delta \bar{P}_t = \int_0^{\Delta s} \rho F_t \, ds \quad (12)$$

meaning the loss of rotating pressure equals the work by the resistance along the streamline Δs that, in differential form, is

$$\rho F_t = \frac{d\bar{P}_t}{ds}$$

The coefficient μ in Eq. (11) can be obtained by

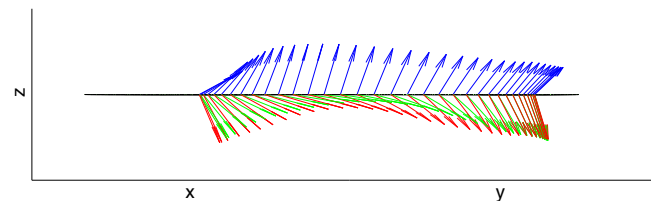


Fig. 3 Vectors of force and velocity in $z - \theta$ plane.

$$\mu = \frac{\Delta \bar{P}_t}{\rho \Delta s v_{\text{rel}}^2} \quad (13)$$

In addition, in Liu et al.'s work [36], the response of the body force can be described as a function of perturbations of flowfield parameters, like $\mathbf{F}' = f(p', v', \rho')$. Thus, it can be described by using a first-order lag equation in cybernetics:

$$\tau \frac{dF'}{dt} + F' = \frac{\partial F}{\partial v_r} v'_r + \frac{\partial F}{\partial v_\theta} v'_\theta + \frac{\partial F}{\partial v_z} v'_z \quad (14)$$

where τ is the time delay constant, which is generally assumed to be on the order of the flowthrough time in the bladed region. By using the transform between stationary coordinates and blade moving coordinates,

$$\left. \frac{\partial}{\partial t} \right|_{\text{blade row}} = \left(\frac{\partial}{\partial t} + \Omega \frac{\partial}{\partial \theta} \right) \Big|_{\text{stationary}}$$

the response of the body force can be obtained as

$$\begin{aligned} \mathbf{F}'_n &= \lambda \begin{bmatrix} (n_r/n_\theta)a_1 & (n_r/n_\theta)a_2 \\ a_1 & a_2 \\ (n_r/n_\theta)a_1 & (n_r/n_\theta)a_2 \end{bmatrix} \Phi', \\ \mathbf{F}'_t &= -2\mu\lambda \begin{bmatrix} v_{0r}v_r & v_{0r}v_{\theta r} & v_{0r}v_z \\ v_{0\theta}v_r & v_{0\theta}v_{\theta r} & v_{0\theta}v_z \\ v_{0z}v_r & v_{0z}v_{\theta r} & v_{0z}v_z \end{bmatrix} \Phi' \end{aligned} \quad (15)$$

where

$$\begin{aligned} \lambda &= \frac{1}{1 + i(\omega + m\Omega)\tau}, \quad \mu = \frac{\bar{P}_{t,b} - \bar{P}_{t,a}}{\rho_a(s_b - s_a)v_{\text{total},a}^2}, \\ \begin{cases} a_1 = k_1 \left[\left(v_{\text{total}} + \frac{v_{\text{total}}^2}{v_{\text{total}}} \right) \tau_\theta - v_{\theta r} \right], \\ a_2 = k_1 v_r \left[\frac{v_{\theta r}}{v_{\text{total}}} \tau_\theta - 1 \right] \end{cases}, \\ k_1 &= \frac{(\partial v_\theta / \partial r) + (v_z/v_r)(\partial v_\theta / \partial z) + (v_\theta/r)}{v_{\text{total}}\tau_\theta - v_{\theta r}} \end{aligned}$$

and where

$$\mathbf{F}' = [0 \quad F'_r \quad F'_\theta \quad F'_z \quad 0], \quad \Phi' = [\rho', p', v'_r, v'_\theta, v'_z]^T$$

B. Computational Models

Two different models are developed herein to predict the stall inception, aimed at giving different ways to calculate this unsteady phenomenon and comparing the accuracy, computation time, and grid point independence of these two models.

1. Meridional Plane Model

To simplify the problem, here, the Euler equation is applied regardless of viscosity and the mean flowfield is circumferentially averaged. Substituting Eq. (15) into Eq. (4), then

$$\left[A \frac{\partial}{\partial r} + C \frac{\partial}{\partial z} + D + i \left(\frac{m}{r} B - \omega T \right) - \mathbf{F}'_n - \mathbf{F}'_t \right] \hat{\Phi} = 0 \quad (16)$$

As the equation is homogeneous, a nontrivial solution of $\hat{\Phi}$, which stands for the perturbation's existence in the flow region, exists only if the determination of the matrix is zero. Thus,

$$\det(Q(\omega)) = 0 \quad (17)$$

where

$$Q(\omega) = A \frac{\partial}{\partial r} + C \frac{\partial}{\partial z} + D + i \left(\frac{m}{r} B - \omega T \right) - \mathbf{F}'_n - \mathbf{F}'_t$$

The spectral technique based on the Chebyshev–Gauss–Lobatto points is implemented in order to tackle the derivatives in $Q(\omega)$. This numerical method, widely adopted in boundary value problems, can improve the precision of the numerical solution and minimize the discrete points for saving computational costs: the application of which was systematically concluded by Pyeret [37] on viscous flow. Hence, a transform that can be generally feasible for any complex flow passage is needed in order to transform the grid from the physical domain (z, r) to the computational domain (ξ, η) so that the grid lines are orthogonal and suitable for the spectrum method (see Fig. 4). Here, a Jacobi transform is applied to make the coordinate transformation, the derivatives of which are

$$\begin{cases} \frac{\partial}{\partial z} = \frac{1}{J} \left(\frac{\partial r}{\partial \eta} \frac{\partial}{\partial \xi} - \frac{\partial r}{\partial \xi} \frac{\partial}{\partial \eta} \right) \approx \frac{1}{J} \left(\frac{\Delta r}{\Delta \eta} \frac{\partial}{\partial \xi} - \frac{\Delta r}{\Delta \xi} \frac{\partial}{\partial \eta} \right) \\ \frac{\partial}{\partial r} = \frac{1}{J} \left(\frac{\partial z}{\partial \xi} \frac{\partial}{\partial \eta} - \frac{\partial z}{\partial \eta} \frac{\partial}{\partial \xi} \right) \approx \frac{1}{J} \left(\frac{\Delta z}{\Delta \xi} \frac{\partial}{\partial \eta} - \frac{\Delta z}{\Delta \eta} \frac{\partial}{\partial \xi} \right) \end{cases} \quad (18)$$

where

$$J = \frac{\partial z}{\partial \xi} \frac{\partial r}{\partial \eta} - \frac{\partial z}{\partial \eta} \frac{\partial r}{\partial \xi}$$

Therefore, the matrix equation is transformed as follows:

$$\left(A' \frac{\partial}{\partial \xi} + C' \frac{\partial}{\partial \eta} + D + i \left(\frac{m}{r} B - \omega T \right) - \mathbf{F}'_n - \mathbf{F}'_t \right) \hat{\Phi} = 0 \quad (19)$$

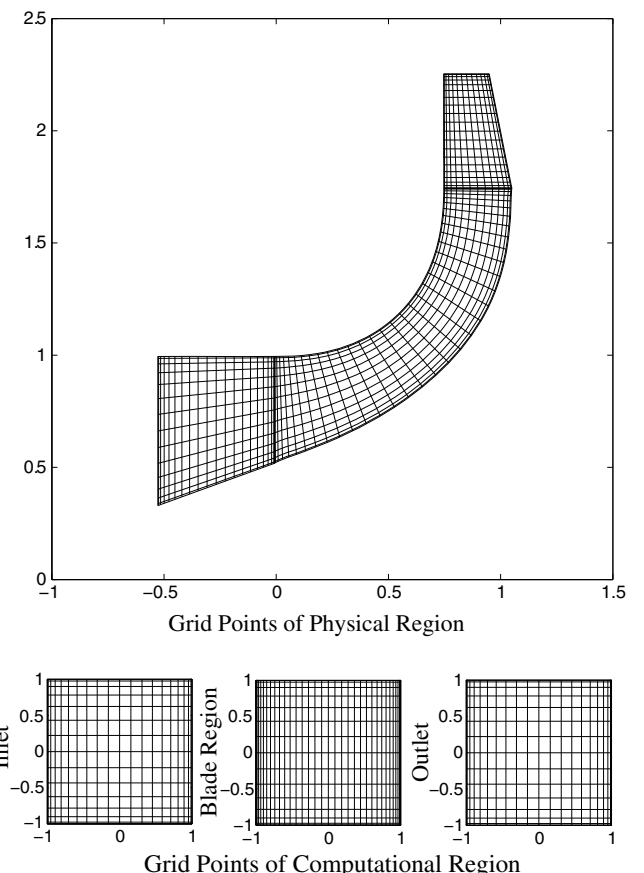


Fig. 4 Transformation of coordinates.

$$A' = \frac{1}{J} \left(-\frac{\Delta z}{\Delta \eta} A + \frac{\Delta r}{\Delta \eta} C \right), \quad C' = \frac{1}{J} \left(\frac{\Delta z}{\Delta \xi} A - \frac{\Delta r}{\Delta \xi} E \right) C \quad (20)$$

The spectral grids satisfy

$$\begin{cases} \xi_i = \cos\left(\frac{\pi i}{N_r}\right), & i = 0, 1, \dots, N_r \\ \eta_j = \cos\left(\frac{\pi j}{N_z}\right), & j = 0, 1, \dots, N_z \end{cases} \quad (21)$$

where $N_r + 1$ and $N_z + 1$ are the total number of nodes in computational coordinates.

2. Normal Expansion Model

To clearly specify the eigenfrequencies during the stall process, a normal expansion model is developed herein. Since the normal direction is approximately the longitudinal direction in the computational domain, it can be obtained that

$$\hat{\Phi} = \hat{\Phi}(\xi) e^{i\omega t} \quad (22)$$

Substituting it into Eq. (19) results in

$$\left(A' \frac{\partial}{\partial \xi} + D + i \left(\frac{m}{r} B + \alpha C' - \omega T \right) - \mathbf{F}'_n - \mathbf{F}'_t \right) \hat{\Phi} = 0 \quad (23)$$

For any matrix equation like

$$\left(X \frac{\partial}{\partial \xi} + Y \right) \mathbf{x} = 0 \quad (24)$$

by using spectrum method, we obtain

$$X \sum_{j=1}^N d_{i,j} \mathbf{x}_j + Y \mathbf{x}_i = 0 \quad (25)$$

where the interval of \mathbf{x} consists of N discrete points, i is the notation of a certain point in this interval, and $d_{i,j}$ is the coefficient of the one-order spectrum method, which can be found in Peyret's book [37], as

$$d_{m,n} = \begin{cases} \frac{c_m}{2c_n} \frac{(-1)^{m+n}}{\sin(\pi m/N)(m+n)\sin(\pi n/N)(-m+n)}, & m \neq n, \quad 0 \leq m \leq \frac{N}{2}, \quad 0 \leq n \leq N \\ \frac{-\cos(\pi m/N)}{2\sin^2(\pi m/N)}, & m = n, \quad 1 \leq m \leq \frac{N}{2}, \quad 1 \leq n \leq N \\ \frac{2N^2+1}{6}, & m = n = 0 \\ -d_{N-m,N-n}, & \frac{N}{2} + 1 \leq m \leq N, \quad 0 \leq n \leq N \end{cases}$$

$$c_k = \begin{cases} 2, & k = 0, \quad N \\ 1, & 1 \leq k \leq N-1 \end{cases} \quad (26)$$

Thus, the discrete forms of Eqs. (19) and (23) are finally derived as

$$A' \sum_{m=1}^M d_{(i,j),(m,j)}^\xi \hat{\Phi}_{m,j} + C' \sum_{n=1}^N d_{(i,j),(i,n)}^\eta \hat{\Phi}_{i,n} + \left[D + i \left(\frac{m}{r} B - \omega T \right) - \mathbf{F}'_n - \mathbf{F}'_t \right] \hat{\Phi}_{i,j} = 0 \quad (27)$$

and

$$A' \sum_{j=1}^M d_{i,j}^\xi \hat{\Phi}_j + \left[D + i \left(\frac{m}{r} B + \alpha C' - \omega T \right) - \mathbf{F}'_n - \mathbf{F}'_t \right] \hat{\Phi}_i = 0 \quad (28)$$

C. Boundary and Match Conditions

To provide boundary conditions for a 3-D instability model, the physical circumstances have to be deeply investigated. It is assumed that all the perturbations are generated in the internal flow of the compressor, which, in other words, means that the upstream and downstream are not disturbed. Three important combinations of perturbations called sound wave, vorticity, and entropy modes were first proposed by Kovásznay [38], who conducted the measurement of these fluctuating quantities in both low-speed flow and high-speed flows in 1955. Chu and Kovásznay [39] gave detailed formulas for the three modes in their first-order form. According to the first-order perturbation theory given in their work, for Euler equations, the three distinctly different types of waves or modes obeyed three independent differential equations and had different propagation features: sound waves propagated in all directions, and vorticity and entropy modes traveled with flow toward the downstream.

Therefore, Li and Sun [19] applied this point of view in a linear Euler equation method; and they assumed that vorticity and entropy disturbances at the inlet boundary were zero, and pressure disturbances at both the inlet and outlet boundaries were zero as impedance boundary conditions. For 3-D boundary conditions, according to Stow et al. [40], the vorticity could be thought of as the sum of two types of vorticity waves; then, we obtain

$$\begin{cases} p' = 0 \\ \frac{\partial v'_z}{\partial z} - \frac{\partial v'_\theta}{\partial r} = 0, \quad \frac{\partial v'_r}{\partial z} - \frac{\partial v'_z}{\partial r} = 0 \\ \frac{r \partial \theta}{\rho' - p'/k} = 0 \end{cases} \quad (29)$$

In addition, what needs much attention is the singularity of the body force at the leading and trailing edges, which can be dealt with using the domain decomposition method. By applying matched asymptotic methods of the inner solution around the airfoil nose and outer region, Rusak and Morris [41] and Rusak [42] tackled the nose singularity for subsonic flow. Liu et al. [36] used the domain decomposition spectral method and divided the flow passage into the blade region and the blade-free region so that the mesh could be locally refined without any singularity. Here, the flow passage of the centrifugal compressor is divided into three domains: inlet, blade, and outlet. Assuming the quantities and relevant derivatives are equal at the boundaries gives the matching conditions, respectively:

$$\left. \frac{\partial \Phi}{\partial z} \right|_{\text{inlet}} = \left. \frac{\partial \Phi}{\partial z} \right|_{\text{blade}}, \quad \left. \frac{\partial \Phi}{\partial r} \right|_{\text{blade}} = \left. \frac{\partial \Phi}{\partial r} \right|_{\text{outlet}} \quad (30)$$

D. Numerical Method

Solving the eigenvalue problem [Eq. (17)] leads to nondimensional complex frequency $\omega = \omega_R + i\omega_I$, the imaginary part of which determines the compressor system is stable with a negative value or unstable with a positive value, and the real part of which represents the rotating frequency of the precursor wave. Two nondimensional coefficients are determined as the relative speed (RS) and the damping factor (DF):

$$\text{RS} = \frac{\omega_R}{m\Omega}, \quad \text{DF} = \frac{\omega_I}{m} \quad (31)$$

Singular value decomposition is applied to obtain the eigenvalue, which was adopted by many researchers on searching the roots for the huge complex matrix. As described by Woodley and Peake [43], SVD is a highly efficient technique to deal with the matrix, which is either singular or numerically close to singular. According to the SVD theory, a condition number of the matrix, which is formally defined as the ratio of the largest and smallest singular values, can show the extent of the singularity: only when the reciprocal of the condition number is zero can the matrix be strictly singular. Nevertheless, as the rounding error is accumulated during the numerical process, the roots of the eigenvalue equation are practically found as long as the reciprocal of the condition number is

significantly smaller than elsewhere, which was demonstrated by Cooper et al.'s work [44].

E. Analytical Model Validation

To validate the numerical model, a two-dimensional resonance problem in annulus duct is calculated here; and Table 1 list the parameters of the annulus duct. The governing equations of linearized small perturbation can be established as

$$\begin{cases} \frac{\partial \rho'}{\partial t} + v_z \frac{\partial \rho'}{\partial z} + \rho \frac{\partial v_r'}{\partial r} + \frac{\rho}{r} \frac{\partial v_\theta'}{\partial \theta} + \rho \frac{\partial v_z'}{\partial z} + \rho \frac{v_r'}{r} = 0 \\ \frac{\partial v_r'}{\partial t} + v_z \frac{\partial v_r'}{\partial z} = -\frac{1}{\rho} \frac{\partial p'}{\partial r} \\ \frac{\partial v_\theta'}{\partial t} + v_z \frac{\partial v_\theta'}{\partial z} = -\frac{1}{\rho r} \frac{\partial p'}{\partial \theta} \\ \frac{\partial v_z'}{\partial t} + v_z \frac{\partial v_z'}{\partial z} = -\frac{1}{\rho} \frac{\partial p'}{\partial z} \\ \left(\frac{\partial}{\partial t} + v_z \frac{\partial}{\partial z} \right) p' - a^2 \left(\frac{\partial}{\partial t} + v_z \frac{\partial}{\partial z} \right) \rho' = 0 \end{cases} \quad (32)$$

Finally, the pressure equation can be obtained by consolidating Eq. (32) as

$$(1-M^2) \frac{\partial^2 p'}{\partial z^2} + \frac{\partial^2 p'}{\partial r^2} + \frac{\partial^2 p'}{\partial r^2} - \frac{1}{a^2} \frac{\partial^2 p'}{\partial t^2} - \frac{2M \partial^2 p'}{a \partial z \partial t} + \frac{1}{r} \frac{\partial p'}{\partial r} = 0 \quad (33)$$

where $M = (v_z/a)$. Assuming

$$p' = \sum \tilde{p} R(r) e^{i(kz+m\theta+\omega t)}$$

and substituting it into Eq. (33) yields

$$x^2 R''(x) + x R'(x) + (x^2 - m^2) R(x) = 0 \quad (34)$$

where

$$x = \lambda r, \quad \lambda^2 = \left(\frac{\omega_n}{a} + k_{mn} M \right)^2 - k_{mn}^2 \quad (35)$$

Equation (34) is an m -order Bessel equation, the solution of which is

$$R(r) = b_{mn} J_m(\lambda_{mn} r) + b'_{mn} N_m(\lambda_{mn} r) \quad (36)$$

where boundary conditions

$$\left. \frac{\partial p'}{\partial r} \right|_{r=r_{1,2}} = \left. \frac{\partial R(x)}{\partial r} \right|_{r=r_{1,2}} = 0$$

are set, in that the radial velocity $v_r' = 0$ on the wall, which gives the equation

$$\left[\begin{array}{cc} \frac{\partial}{\partial r} J_m(\lambda_{mn} r_1) & \frac{\partial}{\partial r} N_m(\lambda_{mn} r_1) \\ \frac{\partial}{\partial r} J_m(\lambda_{mn} r_2) & \frac{\partial}{\partial r} N_m(\lambda_{mn} r_2) \end{array} \right] \left[\begin{array}{c} b_{mn} \\ b'_{mn} \end{array} \right] = 0 \quad (37)$$

To obtain nontrivial solution, the determinant of the coefficient matrix should satisfy

Table 1 Parameters of an annulus duct

Parameter	Value
Temperature	288 K
Pressure	100,000 Pa
Mach number	0.015
Internal radius	0.1826
External radius	0.2487
Length	0.08

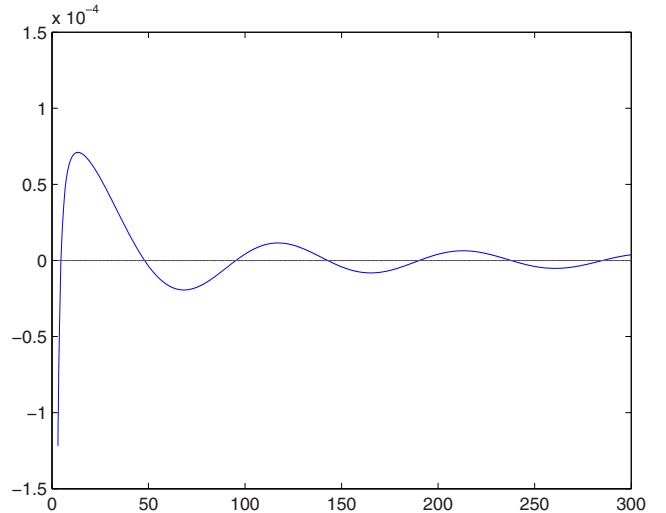


Fig. 5 Roots of the determinant of the coefficient matrix.

$$\begin{vmatrix} \frac{\partial}{\partial r} J_m(\lambda_{mn} r_1) & \frac{\partial}{\partial r} N_m(\lambda_{mn} r_1) \\ \frac{\partial}{\partial r} J_m(\lambda_{mn} r_2) & \frac{\partial}{\partial r} N_m(\lambda_{mn} r_2) \end{vmatrix} = 0 \quad (38)$$

where the eigenvalue λ_{mn} can be obtained by using the function curves in Fig. 5.

In addition, from Eq. (35), we obtain

$$k_{mn}^\pm = \frac{1}{1-M^2} \left(\frac{\omega_n M}{a} \pm \sqrt{\frac{\omega_n^2}{a^2} - (1-M^2)\lambda_{mn}^2} \right) \quad (39)$$

and the inlet and outlet boundary conditions are $p'|_{z=0,L} = 0$. Thus, $k_{mn}^+ = k_{mn}^- + (2\alpha\pi/L)$ is derived and the analytic solution of the resonance frequency can be obtained as

$$\omega_n = a \sqrt{\left[(1-M^2) \frac{\alpha\pi}{L} \right]^2 + (1-M^2)\lambda_{mn}^2} \quad (40)$$

where we set $m = 1$ and obtain the results in Table 2.

Figure 6 verifies that the numerical results rather precisely agree with the analytic solution (the numbers above the black line stand for the circumferential/radial/axial modal number). The grid point independence is also examined, and Fig. 7 shows that sparse points can lead to a fine result due to the high precision of the spectral method.

To test different boundary conditions, we also use two other boundary conditions for the inlet:

$$\begin{cases} p' = 0 \\ \frac{\partial v_r'}{\partial z} - \frac{\partial v_z'}{\partial r} = 0, \quad \frac{\partial v_\theta'}{\partial r} + \frac{v_\theta'}{r} - \frac{\partial v_r'}{\partial \theta} = 0 \\ \rho' - p'/k = 0 \end{cases} \quad (41)$$

$$p' = v'_z = v'_\theta = v'_r = \rho' = 0 \quad (42)$$

but the results are of no grid independence, and only the boundary conditions we provided can meet this requirement. Figures 8 and 9 show the results for boundary conditions (41) and (42), respectively.

Table 2 Resonance frequencies of an annulus duct

α, λ	Analytical result	Numerical result
1,4.7	13,452.34	13,438
1,48.0	21,095.50	21,092
2,4.7	26,761.79	26,621

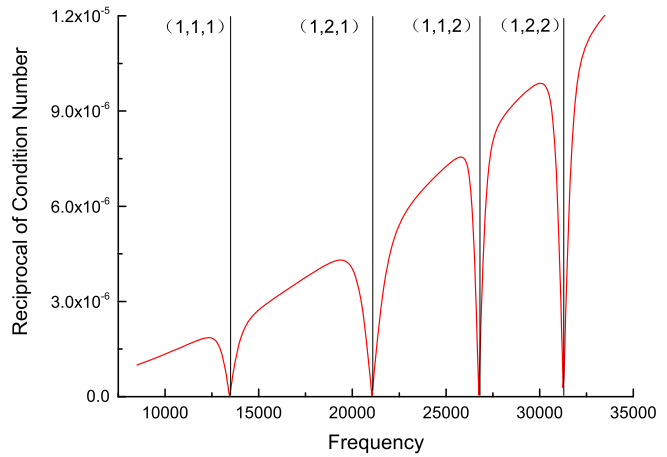
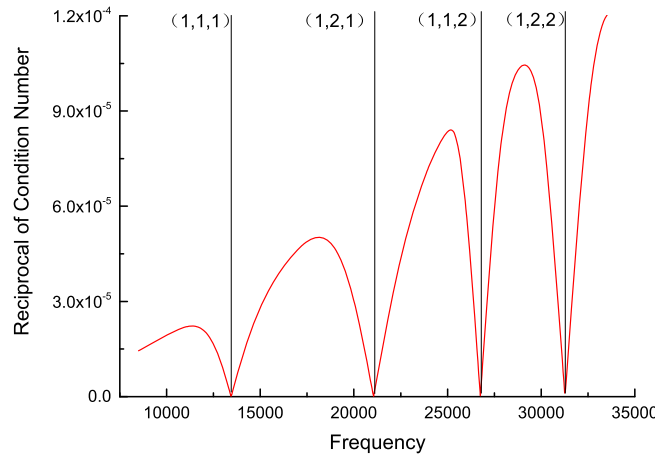


Fig. 6 Numerical and analytical results of resonance frequencies.

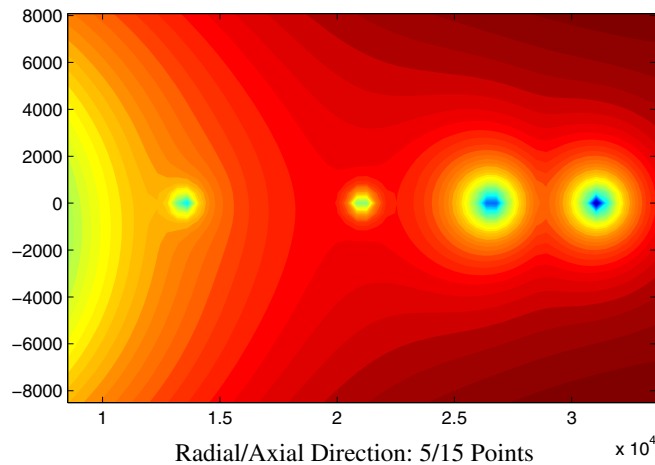


Fig. 7 Grid independence inspection.

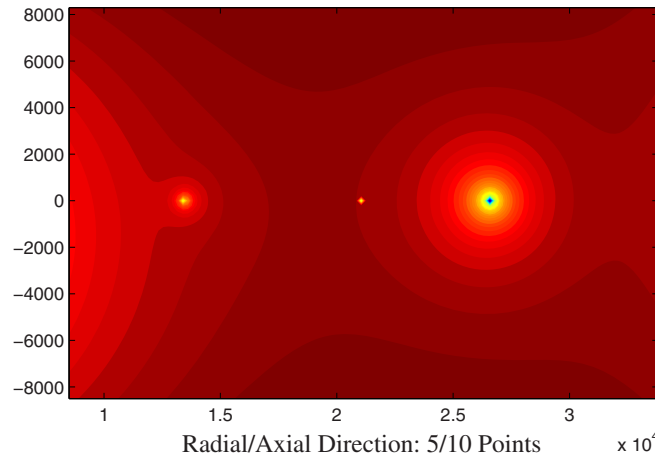
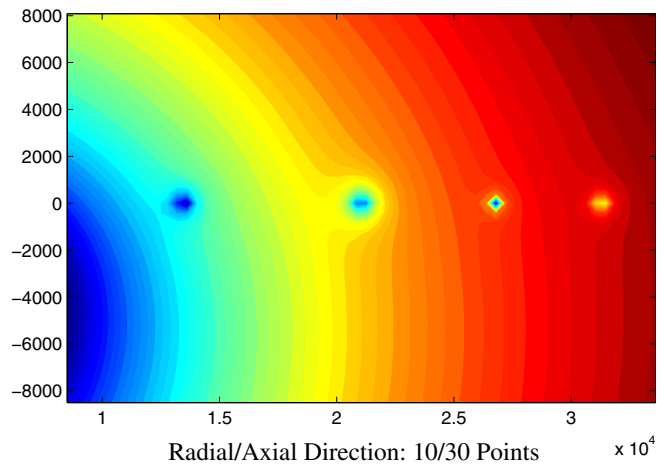


Fig. 8 Distribution of eigenvalues for boundary condition 1.

Obviously, only the original boundary condition has the same result with the analytical eigenvalues, which was also proposed in Stow et al.'s work [40].

III. Validation of Stall Inception Model on a Low-Speed Centrifugal Compressor

In this section, both the meridional model and the normal expansion model will be validated against the prediction of the stall onset of the NASA low-speed centrifugal compressor (LSCC). In 1995, Hathaway et al. [45] used a laser anemometer to survey the

flowfield of the LSCC, and they obtained the detailed parameters of the flow passage, as well as a performance working line. Therefore, the models presented here will be validated with the numerical and experimental study of the LSCC. The major design parameters for the low-speed centrifugal compressor are given in Table 3.

The steady 3-D compressible flowfield in the CFD computation is computed on a total number of approximately 291,000 grid nodes, depicted in Fig. 10, which consist of 153 points in the streamline and 41 points in the blade-to-blade direction and spanwise directions, respectively. The spatial discretization scheme of the algorithm is based on central discretization and upwind discretization,

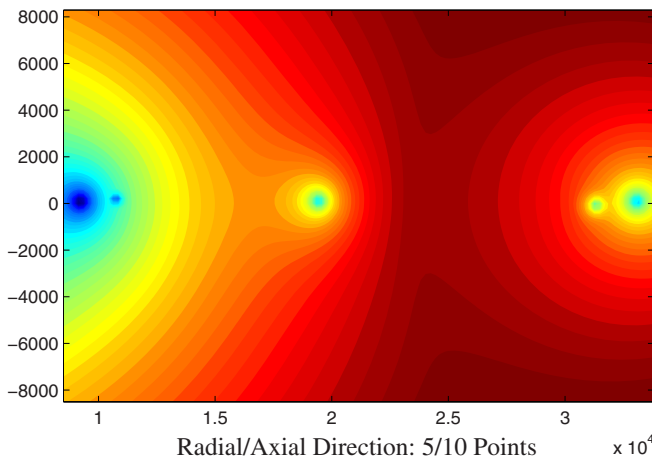


Fig. 9 Distribution of eigenvalues for boundary condition 2.

respectively, coupled with the Spalart–Allmaras turbulence model, multigrid, and local time-stepping technique for convergence.

Essentially, rotating stall, as an unsteady phenomenon, could not be predicted by the numerical convergence of steady calculation because the governing equations of them are totally different. Thus, the model discussed here will give a clear interpretation of the flow instability process in an unsteady point of view. To achieve this goal, several techniques are specified in order to find the solution of eigenvalue equation (17):

1) Set an appropriate complex frequency domain. Practically, according to experimental results [25], the relative speed of the stall precursor in the centrifugal compressor is around 0.6–0.9, so the interval is set as [0.5, 1.5], whereas the interval of the damping factor is normally set to be [−1, 1]. To start with, the coarse grid of the complex plane is applied to roughly find the region of the eigenvalue. Then, a fine grid is used to identify the coordinate of the point.

2) Check out the grid independence of the result and find the changing roots when the flow mass reduces. There are some pseudoroots that change with different grid settings, and some of them may remain when mass flow changes. All of these points should not be considered.

3) Track the largest-damping factor point. Only the point that first and continuously moves across the stable boundary line $y = 0$ is what we seek.

A. One-Hundred-Percent Design Rotating Speed

The comparison of static pressure rise between CFD and experimental results is illustrated in Fig. 11, which indicates that the measured stall point is approximately 15.0 kg/s. By examining the convergence criterion of the global residual (global residual = 10^{-6} , for all cases), it can be verified that the calculating process remains stable even when the mass flow is about 12 kg/s, failing to specify the unsteady point. In fact, this 3-D steady RANS computational method is not suitable for unsteady phenomenon, and it depends

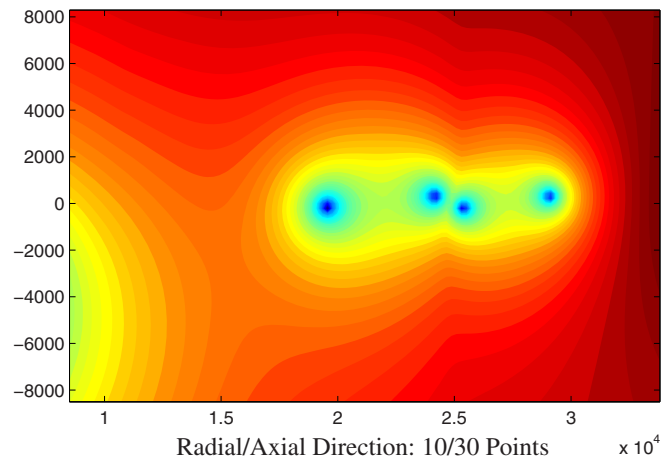


Fig. 10 CFD computational grid.

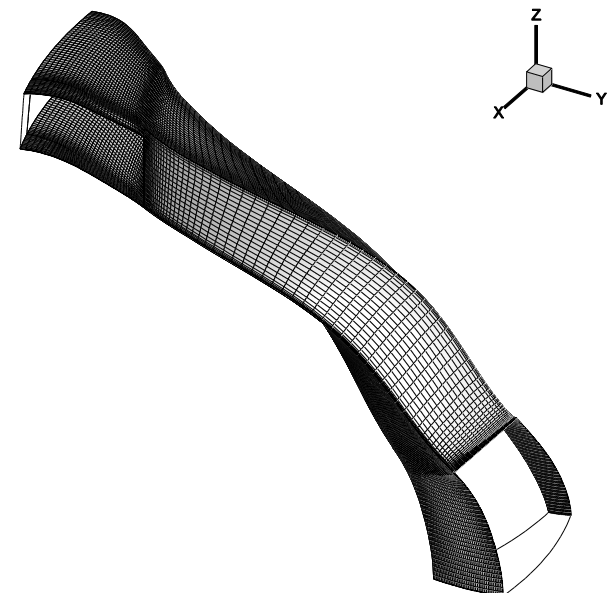


Fig. 11 Comparison of static pressure rise.

greatly on different computation schemes, turbulence models, etc. Therefore, the operation range or stall margin cannot just be judged according to the numerical convergent point of steady flow, which always leads to an optimistic evaluation on the stall margin in the design phase. In contrast, on the basis of the steady data, the unstable point must be determined in terms of the eigenvalue solved by the stability equation.

1. Results of Meridional Plane Model

Here, the steady data are obtained by using central discretization. The root of eigenvalue equations in the proper complex frequency domain is depicted in Fig. 12, where the independence of the grid points is also verified. Accordingly, the number of grid points in the normal direction is set to be 15, whereas the grid numbers in the streamline direction in the inlet, blade, and outlet regions are 21, 35, and 21, respectively. The eigenvalue distribution of the first circumferential mode in the complex frequency domain is illustrated in Fig. 13. Figure 14 indicates that the damping factor increases gradually with the impeller approaching stall, and it changes from negative to positive at 15.6 kg/s first for mode 1, which means that this mode is the main factor causing the imminent instability. The relative speed seems to have a downward trend throughout the rotating process. After the damping factor has become positive, it is around 0.93 for mode 1, which is slightly lower than the rotating speed. Frigne and Van den Braembussche [46], using hot-wire

Table 3 Design parameters for the LSCC (impeller)

Parameter	Value
Mass flow rate	30 kg/s
Rotational speed	1826 rpm
Total pressure ratio	1.173
Estimated efficiency	0.934
Inlet hub-tip radius ratio	0.5
Inlet span	22.042 cm
Inlet tip radius	42.939 cm
Exit radius	76.200 cm
Exit blade height	13.740 cm
Number of blades	20
Inlet tip relative Mach number	0.31
Exit absolute Mach number	0.29

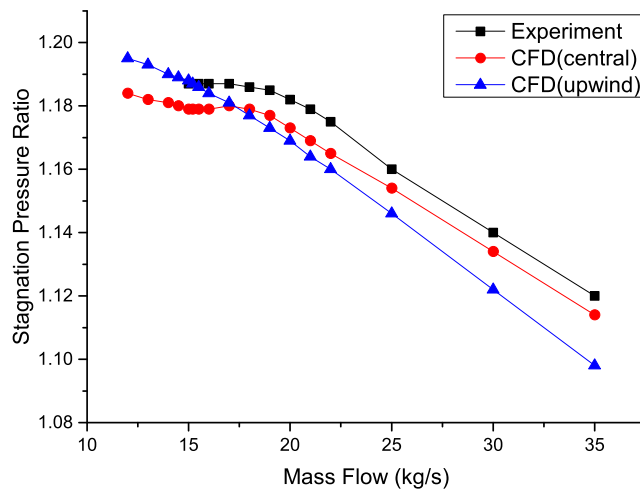


Fig. 11 Characteristics of the LSCC impeller at 100% design rotational speed.

anemometry, found that the propagation speed of a progressive impeller rotating stall due to flow separation is very high and varies between 0.50 and 0.80 rotor rotational frequencies. Thus, for the disturbance speed, the computed figure (0.93) is reasonable. The relative speeds for all the three modes drop considerably in the after-

stall process, which indicates the rotating speed of small disturbances is much faster than that of stalls. Therefore, such results provide a clear disturbance-to-stall changing process: with throttling carrying on, fast rotating disturbances gradually moderate their speed and develop into fully developed stalls. The relative error between the predicted stall inception point and the measured instability point is 4%.

Figure 15 verifies the influence of steady data, where the damping factor changing processes are nearly the same between 22 and 14 kg/s, despite the fact that both the relative speed and damping factor vary between these two different steady results at the beginning and end of the throttling process. Numerical result shows that the stall onset point is 15.6 kg/s for the central discretization scheme and 15.8 kg/s for the upwind discretization scheme. Their relative errors are 4 and 5.3%, respectively, validating that the meridional model can be adopted to predict stall inception with reasonable precision.

To verify the influence of the body force model, we added contrast numerical cases (model 1 is original): model 2 uses a different drag force formula and takes density disturbances into consideration:

$$\mathbf{F}_t = \mu \frac{\mathbf{v}_r^2}{\rho} \quad (43)$$

Therefore, the perturbation forms of these body forces become

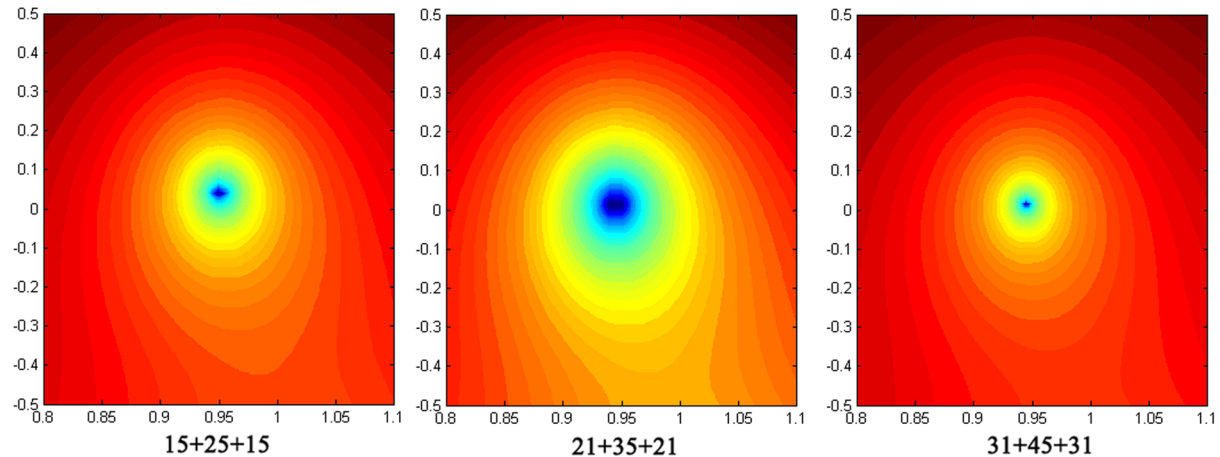


Fig. 12 Roots of eigenvalue equation for different grids (streamline points in inlet, blade, and outlet region: 15 + 25 + 15, 21 + 35 + 21, and 31 + 45 + 31).

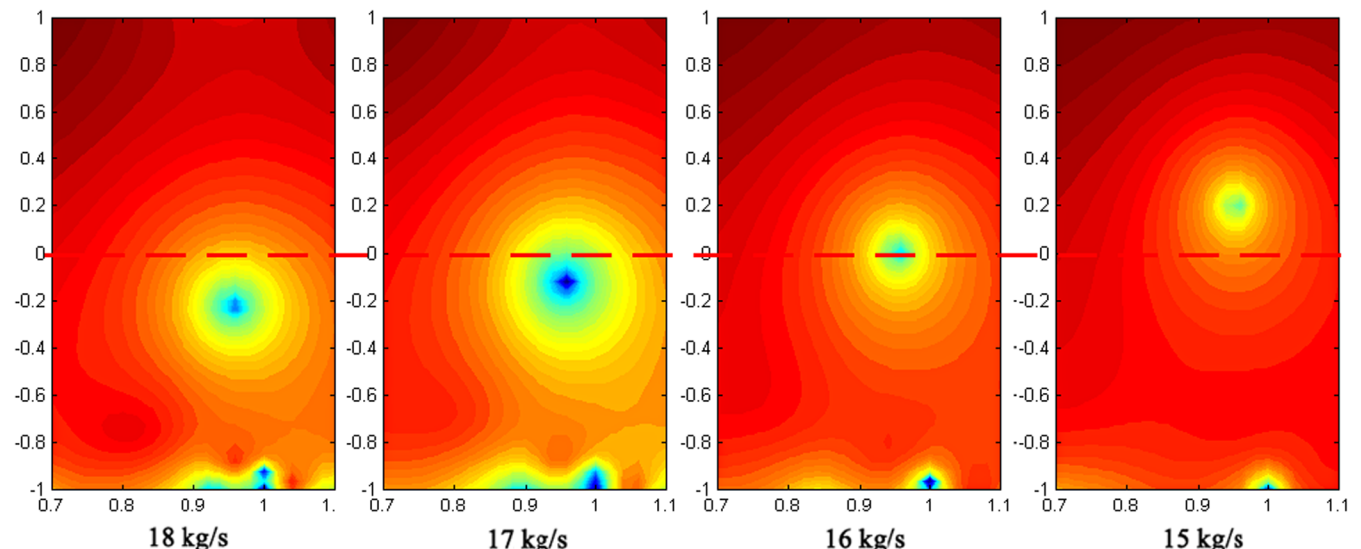
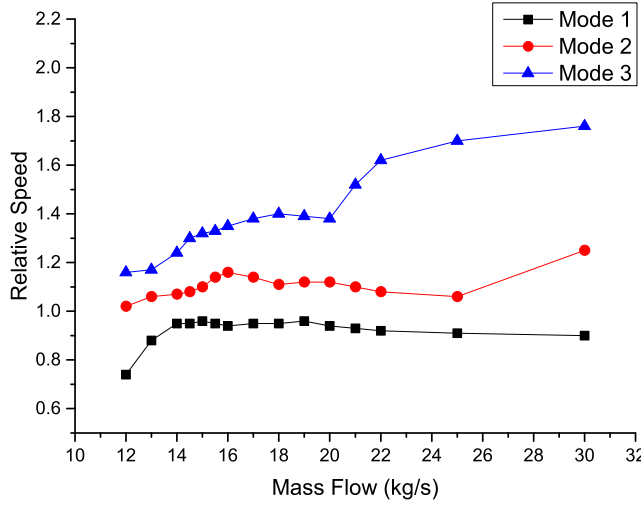
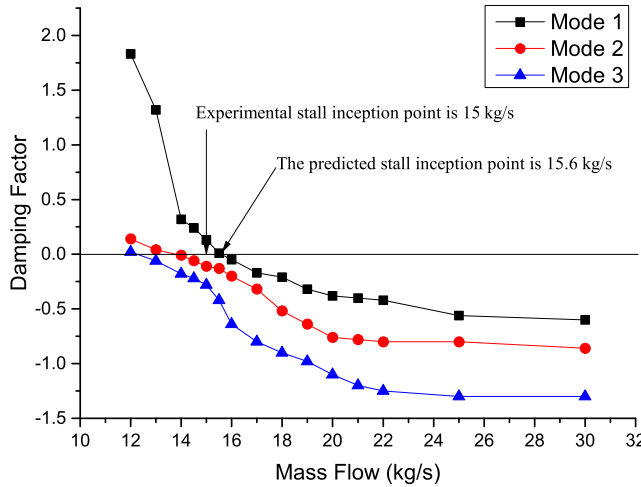


Fig. 13 Eigenvalues in complex frequency domain.

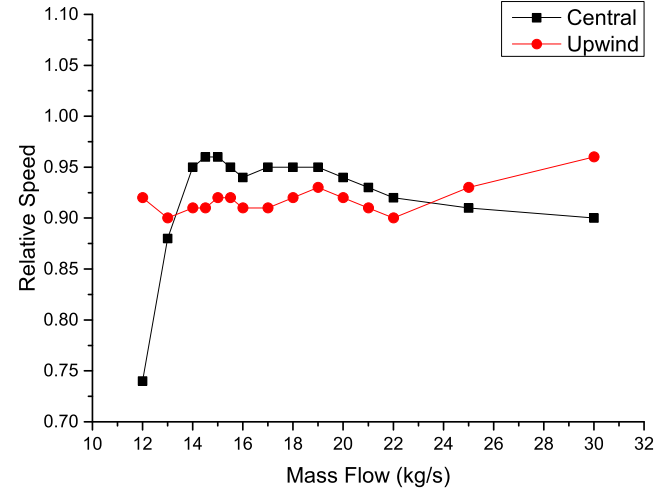


a) Relative speed

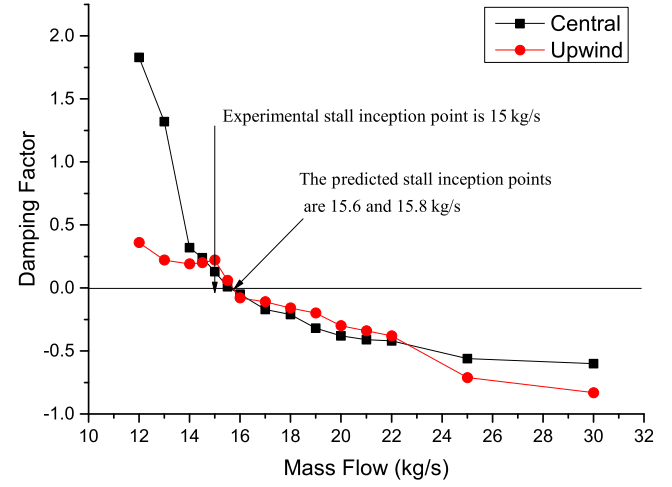


b) Damping factor

Fig. 14 Computed eigenvalues at 100% speed.



a) Relative speed



b) Damping factor

Fig. 15 Computed eigenvalues of central and upwind schemes.

Model 2:

$$\begin{aligned} \mathbf{F}'_n &= \lambda \begin{bmatrix} (n_r/n_\theta)a_1 & (n_r/n_\theta)a_2 \\ a_1 & a_2 \\ (n_r/n_\theta)a_1 & (n_r/n_\theta)a_2 \end{bmatrix} \Phi', \\ \mathbf{F}'_t &= -2\mu\lambda \begin{bmatrix} v_{\text{total}}^2/(2\rho^2) & v_{0r}v_r & v_{0r}v_{\theta r} & v_{0r}v_z \\ v_{\text{total}}^2/(2\rho^2) & v_{0\theta}v_r & v_{0\theta}v_{\theta r} & v_{0\theta}v_z \\ v_{\text{total}}^2/(2\rho^2) & v_{0z}v_r & v_{0z}v_{\theta r} & v_{0z}v_z \end{bmatrix} \Phi' \quad (44) \end{aligned}$$

where

$$\begin{aligned} \lambda &= \frac{1}{1 + i(\omega + m\Omega)\tau}, \quad \mu = \frac{\bar{P}_{t,b} - \bar{P}_{t,a}}{(s_b - s_a)v_{\text{total},a}^2}, \\ \left\{ \begin{array}{l} a_1 = k_1 \left[\left(v_{\text{total}} + \frac{v_r^2}{v_{\text{total}}} \right) \tau_\theta - v_{\theta r} \right], \\ a_2 = k_1 v_r \left[\frac{v_{\theta r}}{v_{\text{total}}} \tau_\theta - 1 \right] \end{array} \right. , \\ k_1 &= \frac{(\partial v_{\theta r}/\partial r) + (v_z/v_r)(\partial v_{\theta r}/\partial x) + (v_{\theta r}/r)}{v_{\text{total}}\tau_\theta - v_{\theta r}} \end{aligned}$$

Figure 16 shows the damping factor and the relative speed of these different body force models, and it is clear that both the relative speed

and damping factor are almost the same when near the critical point. This is probably because it is a low-speed compressor system, and the model may take effect on a high-speed system. The changing processes are also presented in Fig. 17.

It is true that these body force models are empirical to a certain degree, but the comparison indicates that, as long as the model satisfies the momentum and the energy conservation laws, the predicting result is reasonable. The response form of the body force model describes its response to the perturbations of density, velocity, and pressure; contains the geometry of the blade force; and reflects the physical laws of the interaction between the blades and the flow. Thus, it is reliable to derive the body force models in the way we proposed, which was also used in Gordon's [20] and Gong et al.'s work [34] in certain ways.

2. Results of Normal Expansion Model

Three normal modes [$\alpha = 1, 2, 3$ in Eq. (23), circumferential mode $m = 1$] are focused on. It is found that the normal direction grid points can be reduced to nine (illustrated in Fig. 18), which greatly decreases the whole grid number and the dimension of the matrix. Figure 19b shows that, with throttling carrying on, the damping factor of mode 1 increases gradually and changes first from negative to positive when the mass flow is approximately 16.0 kg/s. In addition, the relative speed of the most unstable mode at stall inception here is around 0.68, within the measured dominant instability frequency range, and validates the prediction accuracy of the proposed model.

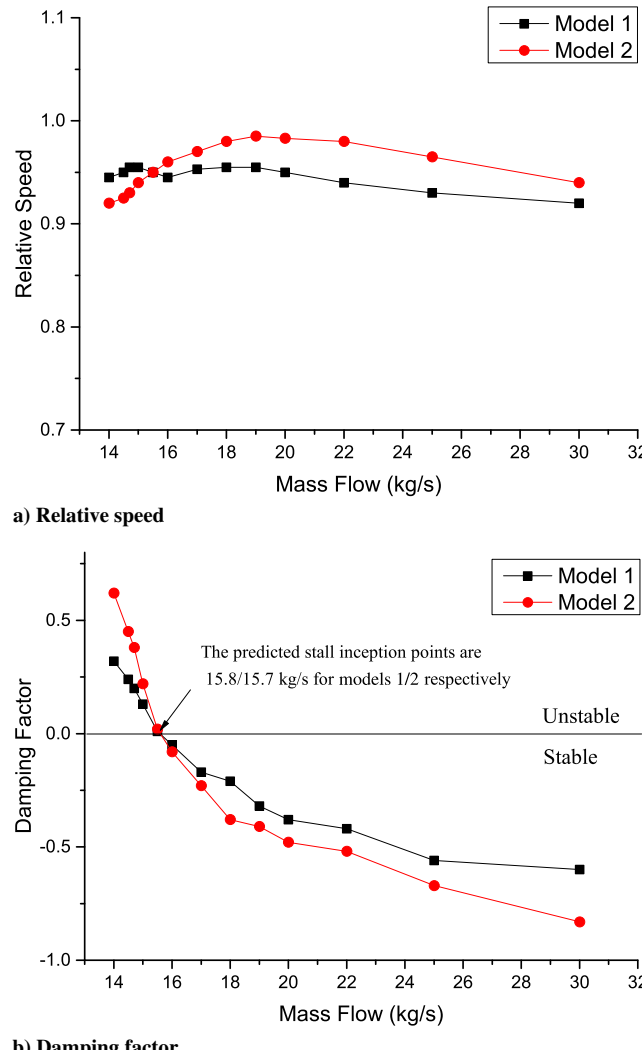


Fig. 16 Computed eigenvalues of different body force models.

B. Seventy-Five-Percent Design Rotating Speed

1. Results of Meridional Plane Model

The stall onset point for the 75% rotating speed is also predicted here. Figure 20 shows its stagnation pressure ratio curve, indicating it remains stable even at 6 kg/s. With throttling carrying on, the damping factor in Fig. 21b increases gradually and changes from negative to positive when the mass flow is around 16.0 kg/s. The

relative speed of the most unstable mode at stall inception is around 0.68.

2. Results of Normal Expansion Model

In terms of the results of the expansion model, the relative speed (0.88) seems a little higher than that of the meridional plane model (0.77) at a 75% rotating speed, as shown in Fig. 22a. The predicted stall inception point specified by the damping factor in Fig. 22b would be 10.9 kg/s, which is slightly higher than the result provided by the meridional plane model. However, due to lack of experimental data for stall onset at the 75% rotating speed, the comparison with experimental results is not available. The computation times using these two models are listed in Table 4, which indicates that the normal expansion model can be more efficient to predict the stall inception within an acceptable accuracy.

IV. Analysis and Discussion on the Proceeding Results

Overall, global stability analysis has become a hot topic in various flow stability problems [12,13]. This is also attributed to a clear stability criterion with which the approach can be provided without sacrificing the complex flow and geometry involved. However, the existing approach for global stability analysis is generally used to handle the stability issues like flow transition and aircraft buffet boundary under the assumption of free or semifree space; the relevant stabilities are mainly associated with the Reynolds number and velocity profile. In contrast, the flow stability like stall inception in turbomachinery is mainly caused by the fluctuations of the blade or impeller loading in addition to inhomogeneous steady flow in three directions. Therefore, the key step toward establishing such a model is how to describe the function of unsteady loading on a blade. In consideration of Sirovich's famous proof that any immersed body in fluids can be replaced by a generalized function [23], the role of a blade can be merged into the momentum equation as a source term, whereas the source term must be related to various state variables like density, pressure, and velocity. Therefore, a stability equation in the form of a matrix can be strictly established, the eigenvalue solution of which can be considered as a stability criterion for stall inception in turbomachinery.

In principle, the present model can theoretically be used to handle the arbitrarily complex flow and geometry for the stability problem in turbomachinery. However, for practical application, some further simplification has to be implemented. In fact, the two reduced-order models in the present work are a kind of attempt to capture the main physics of stall inception in a centrifugal compressor with acceptable computational costs. Particularly, the actual meridional geometry of the impeller in Fig. 2 is represented; it is very useful to study the relationship between the operation range or stall margin and the variation of sweep and the skewing blade in the design phase. From the results as shown in Fig. 14, it seems the present model can make a

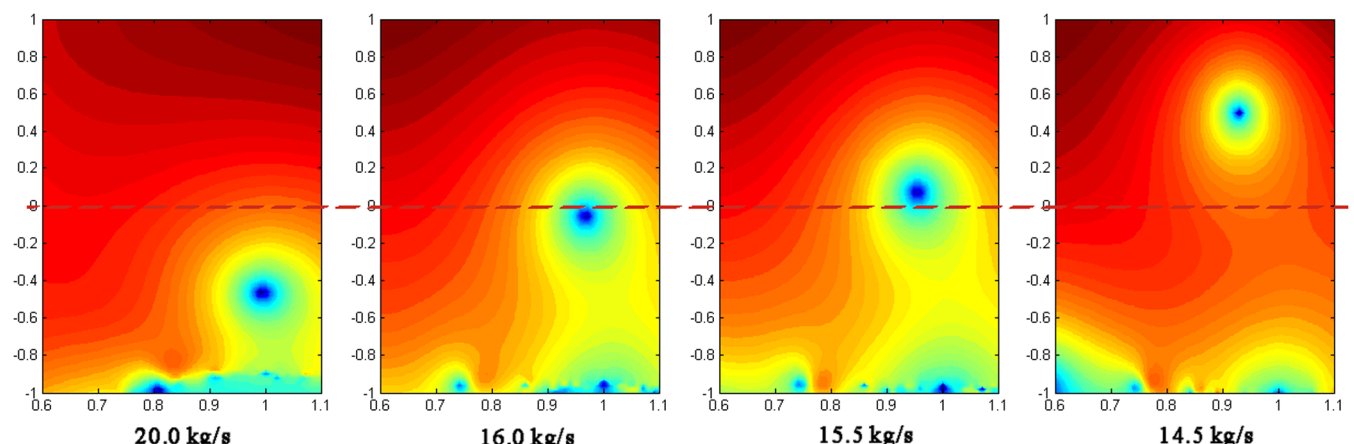


Fig. 17 Changing process of eigenvalue for model 2.

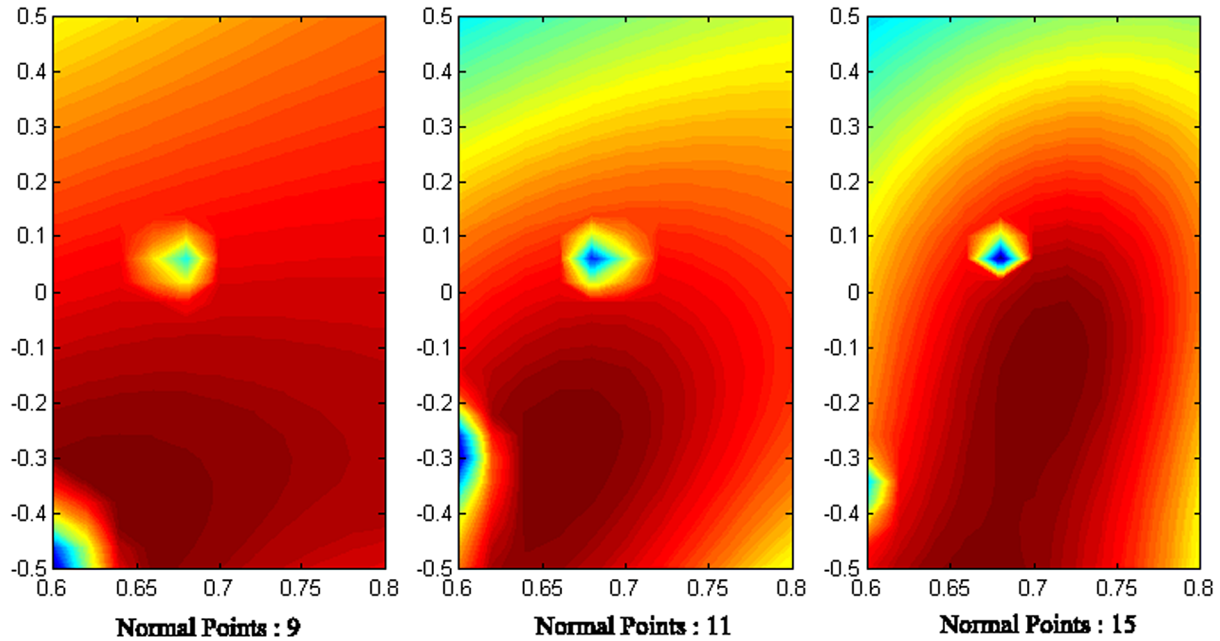
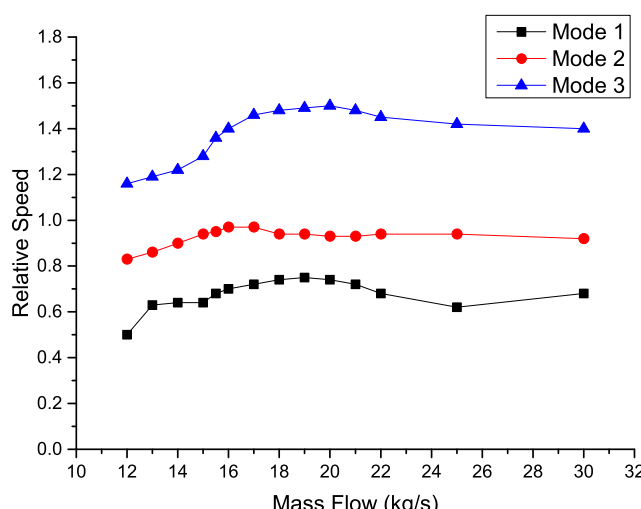
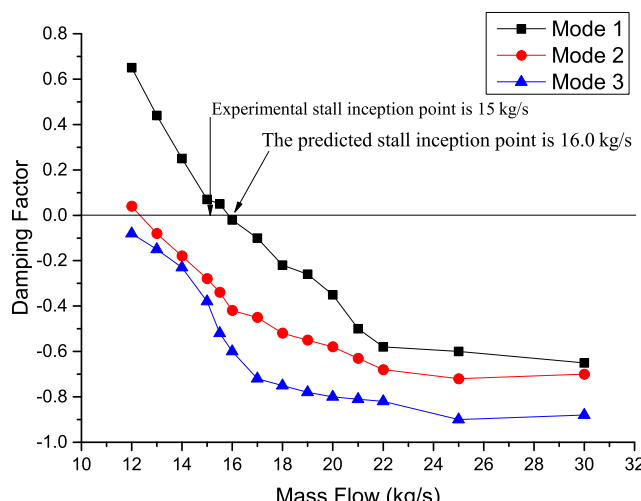


Fig. 18 Grid independence inspection (points in normal direction: 9, 11, and 15).



a) Relative speed



b) Damping factor

Fig. 19 Computed eigenvalues at 100% speed.

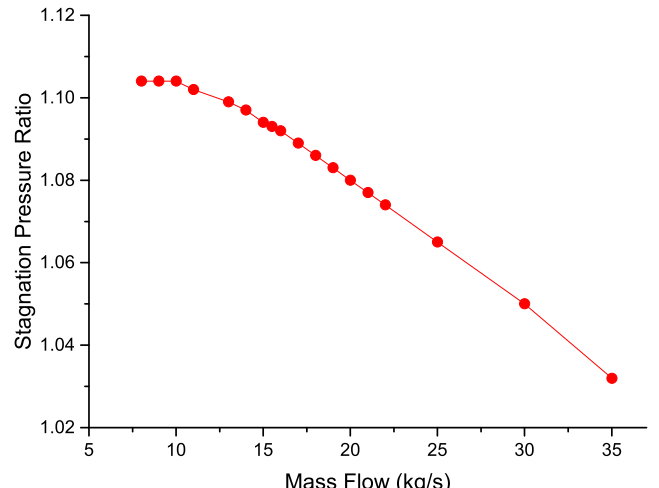
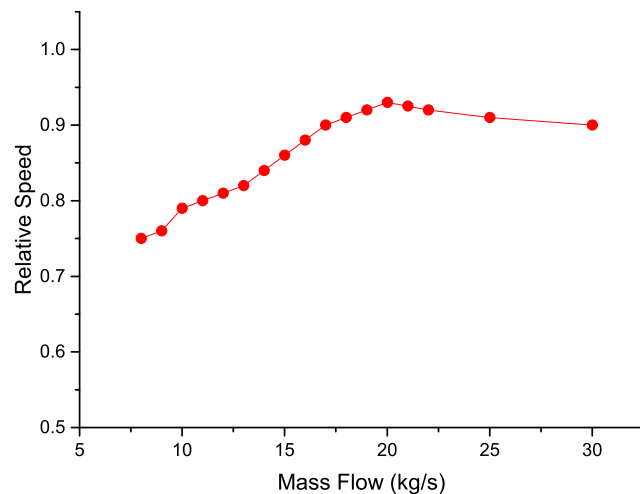


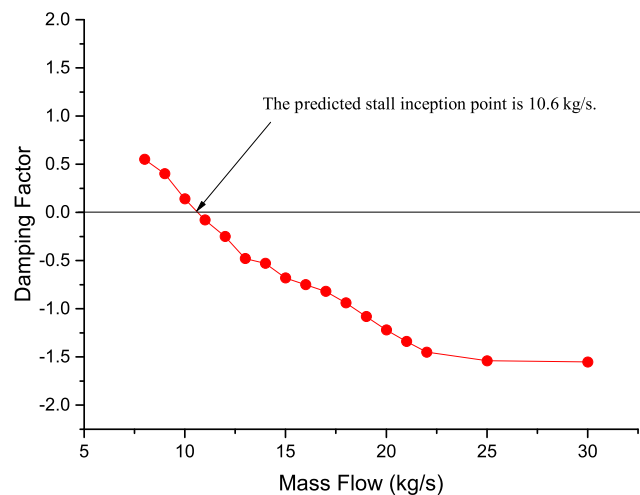
Fig. 20 Characteristics of the LSCC impeller at 75% design rotational speed.

relatively good prediction for the critical point in comparison with the experimental data. However, the predicted circumferential propagation speed in Fig. 14 has an error over 15% [46]. This difference may come from the assumption of the circumferentially averaged flow. The present model only includes the effect of two inhomogeneous steady flows in the both axial and radial directions, whereas the inhomogeneous flow in the circumferential direction may have a nonnegligible influence on the propagation speed in this direction. Therefore, if the nonuniformity in the circumferential steady flow is included in the model, the prediction of the propagation speed can be improved.

On the other hand, the body force model is also a crucial factor to affect the predicting results. This requires that the unsteady loading on the blade has a right physical response to any perturbations. In fact, how to apply the conservation laws to give more reasonable loading distribution on the blade still needs further investigation, especially on the impeller with transonic flow and complex flow in a multistage compressor environment. The progress in this aspect can also advance the predicting accuracy.



a) Relative speed



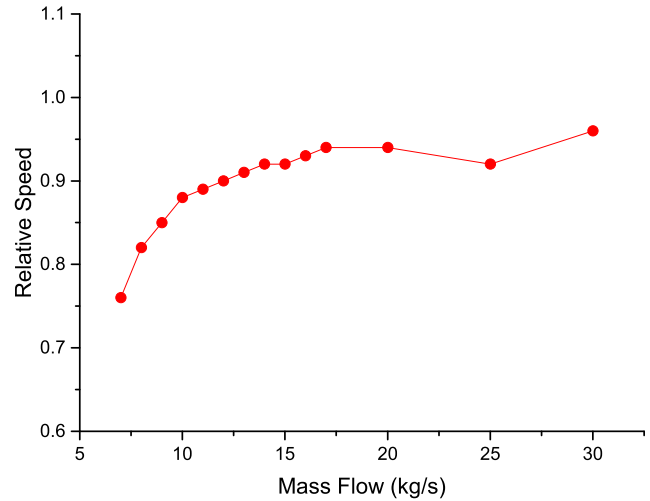
b) Damping factor

Fig. 21 Computed eigenvalues of different rotating speeds.

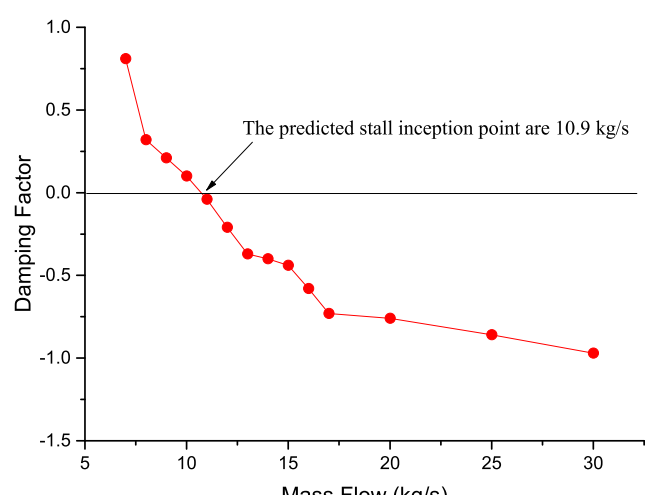
Finally, the computational method of the eigenvalue is always a challenge in global stability analysis. The current algorithms deal with QR , QZ decomposition or Jacobi methods and the method based on calculation of the invariant subspaces having dimensions significantly smaller than the original problem. In this work, the relevant eigenvalue calculation has been presented on the basis of the singular value decomposition, along with the application of the spectral method. However, if we use spectral method to disperse the derivative terms in 3-D N-S equations, it still uses a huge amount of computing resources due to the enormous matrix. Thus, besides the SVD method, new numerical techniques for matrix decomposition also need to be developed urgently.

Table 4 Computation results of the two models (four CPUs at 4.00 GHz)

Model	Meridional	Normal expansion
Stall inception point, kg/s	15.2	15.1
Number of grid points	1035	483
Computation time of every frequency point, s	103	11
Computation time of every mass flow point (500 frequency points), h	14.3	3.25
Computation time of total working line d (30 ~ 14 kg/s, ≈ 10 points)	6.0	1.4



a) Relative speed



b) Damping factor

Fig. 22 Computed eigenvalues of different rotating speed.

V. Conclusions

This paper presents a stall inception model of centrifugal compressors based on a global stability method. The two important elements (i.e., a body force model suitable for a centrifugal impeller and the computational method of an eigenvalue) are addressed in this work. By applying the immersed boundary method, a body force model that follows the conservation laws for momentum and energy is applied here to simulate the effect of blades, which gives a clear understanding on its physical meaning with a detailed geometry profile. Additionally, the boundary conditions, as a significant factor for the eigenvalue problem, are carefully set up and analyzed according to the linearized disturbances theory in order to obtain a real physical solution. On the basis of these advancements, two numerical models for the prediction of stall inception in a centrifugal compressor are developed and compared in this paper. To numerically calculate the stability equation using the spectral method, a high-precision computing method, called the Jacobi transform, is applied to obtain a discrete equation.

It can be concluded that both of these models are capable of predicting stall inception of a low-speed centrifugal compressor with an acceptable relative error. The stability model developed in this paper can provide an unambiguous judgment on stall inception without numerical requirement, empirical relations of loss, and deviation angle. This approach can be applied as a useful tool to check the overestimated stall margin during the design phase of centrifugal compressors. In addition, the normal expansion model costs a short time of few minutes and is efficient for industrial application.

Acknowledgments

This work is supported by the National Natural Science Foundation of China (grant nos. 51406229, 51236001, and 51576008), the National Basic Research Program of China (grant no. 2012CB720201), the Aeronautical Science Foundation of China (2014ZB51018), the Collaborative Innovation Center for Advanced Aero-Engine of China, and the Fundamental Research Funds for the Central Universities.

References

- [1] Ffowcs Williams, J., and Huang, X., "Active Stabilization of Compressor Surge," *Journal of Fluid Mechanics*, Vol. 204, July 1989, pp. 245–262.
doi:10.1017/S0022112089001746
- [2] Stein, A., Niazi, S., and Sankar, L. N., "Computational Analysis of Centrifugal Compressor Surge Control Using Air Injection," *Journal of Aircraft*, Vol. 38, No. 3, 2001, pp. 513–520.
doi:10.2514/2.2791
- [3] Rodgers, C., "Impeller Stalling as Influenced by Diffusion Limitations," *Journal of Fluids Engineering*, Vol. 99, No. 1, 1977, pp. 84–93.
doi:10.1115/1.3448569
- [4] Kammer, N., and Rautenberg, M., "A Distinction between Different Types of Stall in a Centrifugal Compressor Stage," *Journal of Engineering for Gas Turbines and Power*, Vol. 108, No. 1, 1986, pp. 83–92.
doi:10.1115/1.323980
- [5] Kyrtatos, N., and Watson, N., "Application of Aerodynamically Induced Prewhirl to a Small Turbocharger Compressor," *Journal of Engineering for Power*, Vol. 102, No. 4, 1980, pp. 943–950.
doi:10.1115/1.3230365
- [6] Spakovszky, Z., "Backward Traveling Rotating Stall Waves in Centrifugal Compressors," *ASME Turbo Expo 2002: Power for Land, Sea, and Air*, American Soc. of Mechanical Engineers, Fairfield, NJ, 2002, pp. 529–543.
doi:10.1115/1.1643382
- [7] Frigne, P., and Van den Braembussche, R., "A Theoretical Model for Rotating Stall in the Vaneless Diffuser of a Centrifugal Compressor," *Journal of Engineering for Gas Turbines and Power*, Vol. 107, No. 2, 1985, pp. 507–513.
doi:10.1115/1.3239589
- [8] Senoo, Y., and Kinoshita, Y., *Limits of Rotating Stall and Stall in Vaneless Diffusers of Centrifugal Compressors*, Vol. 78, American Soc. of Mechanical Engineers, Fairfield, NJ, 1978, Paper V01AT01A019.
- [9] Tan, C., Day, I., Morris, S., and Wadia, A., "Spike-Type Compressor Stall Inception, Detection, and Control," *Annual Review of Fluid Mechanics*, Vol. 42, Dec. 2010, pp. 275–300.
doi:10.1146/annurev-fluid-121108-145603
- [10] Stein, A., Niazi, S., and Sankar, L. N., "Numerical Analysis of Stall and Surge in a High-Speed Centrifugal Compressor," *38th Aerospace Sciences Meeting and Exhibit*, AIAA Paper 2000-0226, 2000.
doi:10.2514/6.2000-226
- [11] Chen, J., Webster, R. S., Hathaway, M. D., Herrick, G. P., and Skoch, G. J., "Numerical Simulation of Stall and Stall Control in Axial and Radial Compressors," *AIAA Paper 2006-0418*, 2006.
doi:10.2514/6.2006-418
- [12] Theofilis, V., "Advances in Global Linear Instability Analysis of Nonparallel and Three-Dimensional Flows," *Progress in Aerospace Sciences*, Vol. 39, No. 4, 2003, pp. 249–315.
doi:10.1016/S0376-0421(02)00030-1
- [13] Gómez, F., Clainche, S. L., Paredes, P., Hermanns, M., and Theofilis, V., "Four Decades of Studying Global Linear Instability: Progress and Challenges," *AIAA Journal*, Vol. 50, No. 12, 2012, pp. 2731–2743.
doi:10.2514/1.J051527
- [14] Zebib, A., "Stability of Viscous Flow Past a Circular Cylinder," *Journal of Engineering Mathematics*, Vol. 21, No. 2, 1987, pp. 155–165.
doi:10.1007/BF00127673
- [15] Rodriguez, D., and Theofilis, V., "Structural Changes of Laminar Separation Bubbles Induced by Global Linear Instability," *Journal of Fluid Mechanics*, Vol. 655, July 2010, pp. 280–305.
doi:10.1017/S0022112010000856
- [16] Rodríguez, D., and Theofilis, V., "On the Birth of Stall Cells on Airfoils," *Theoretical and Computational Fluid Dynamics*, Vol. 25, Nos. 1–4, 2011, pp. 105–117.
doi:10.1007/s00162-010-0193-7
- [17] Crouch, J., Garbaruk, A., Magidov, D., and Travin, A., "Origin of Transonic Buffet on Aerofoils," *Journal of Fluid Mechanics*, Vol. 628, June 2009, pp. 357–369.
doi:10.1017/S0022112009006673
- [18] Yamouni, S., Sipp, D., and Jacquin, L., "Interaction between Feedback Aeroacoustic and Acoustic Resonance Mechanisms in a Cavity Flow: A Global Stability Analysis," *Journal of Fluid Mechanics*, Vol. 717, Feb. 2013, pp. 134–165.
doi:10.1017/jfm.2012.563
- [19] Li, L., and Sun, X., "Effect of Vorticity Waves on Azimuthal Instabilities in Annular Chambers," *Combustion and Flame*, Vol. 162, No. 3, 2015, pp. 628–641.
doi:10.1016/j.combustflame.2014.09.011
- [20] Gordon, K. A., "Three-Dimensional Rotating Stall Inception and Effects of Rotating Tip Clearance Asymmetry in Axial Compressors," Ph.D. Thesis, Massachusetts Inst. of Technology, Cambridge, MA, 1999.
- [21] Paduano, J. D., Greitzer, E., and Epstein, A., "Compression System Stability and Active Control," *Annual Review of Fluid Mechanics*, Vol. 33, No. 1, 2001, pp. 491–517.
- [22] Sun, X., Liu, X., Hou, R., and Sun, D., "A General Theory of Flow-Instability Inception in Turbomachinery," *AIAA Journal*, Vol. 51, No. 7, 2013, pp. 1675–1687.
doi:10.2514/1.J052186
- [23] Sirovich, L., "Initial and Boundary Value Problems in Dissipative Gas Dynamics," *Physics of Fluids*, Vol. 10, No. 1, 1967, pp. 24–34.
doi:10.1063/1.1761987
- [24] Peskin, C. S., "The Immersed Boundary Method," *Acta Numerica*, Vol. 11, Jan. 2002, pp. 479–517.
doi:10.1017/S0962492902000077
- [25] Lawless, P. B., and Fleeter, S., "Rotating Stall Acoustic Signature in a Low-Speed Centrifugal Compressor: Part 1—Vaneless Diffuser," *Journal of Turbomachinery*, Vol. 117, No. 1, 1995, pp. 87–96.
- [26] Spakovszky, Z., and Roduner, C., "Spike and Modal Stall Inception in an Advanced Turbocharger Centrifugal Compressor," *Journal of Turbomachinery*, Vol. 131, No. 3, 2009, Paper 031012.
doi:10.1115/1.2988166
- [27] Zhong, X., "A New High-Order Immersed Interface Method for Solving Elliptic Equations with Imbedded Interface of Discontinuity," *Journal of Computational Physics*, Vol. 225, No. 1, 2007, pp. 1066–1099.
doi:10.1016/j.jcp.2007.01.017
- [28] Lee, L., and LeVeque, R. J., "An Immersed Interface Method for Incompressible Navier-Stokes Equations," *SIAM Journal on Scientific Computing*, Vol. 25, No. 3, 2003, pp. 832–856.
doi:10.1137/S1064827502414060
- [29] Liang, A., Jing, X., and Sun, X., "Constructing Spectral Schemes of the Immersed Interface Method Via a Global Description of Discontinuous Functions," *Journal of Computational Physics*, Vol. 227, No. 18, 2008, pp. 8341–8366.
doi:10.1016/j.jcp.2008.05.020
- [30] Marble, F. E., "Three-Dimensional Flow in Turbomachines," *High Speed Aerodynamics and Jet Propulsion*, Vol. 10, Jan. 1964, pp. 83–166.
- [31] Goldstein, D., Handler, R., and Sirovich, L., "Modeling a No-Slip Flow Boundary with an External Force Field," *Journal of Computational Physics*, Vol. 105, No. 2, 1993, pp. 354–366.
doi:10.1006/jcph.1993.1081
- [32] Longley, J. P., "Calculating the Flowfield Behaviour of High-Speed Multi-Stage Compressors," *ASME 42nd International Gas Turbine and Aeroengine Congress and Exhibition*, American Soc. of Mechanical Engineers Paper 97-GT-468, Fairfield, NJ, 1997,
doi:10.1115/97-GT-468
- [33] Chima, R. V., "A Three-Dimensional Unsteady Cfd Model of Compressor Stability," *ASME Turbo Expo 2006: Power for Land, Sea, and Air*, American Soc. of Mechanical Engineers, Fairfield, NJ, 2006, pp. 1157–1168.
doi:10.1115/GT2006-90040
- [34] Gong, Y., Greitzer, E., Tan, C., and Gordon, K., "A Computational Model for Short-Wavelength Stall Inception and Development in Multistage Compressors," *Journal of Turbomachinery*, Vol. 121, No. 4, 1999, pp. 726–734.
doi:10.1115/1.2836726
- [35] Hill, P. G., and Peterson, C. R., *Mechanics and Thermodynamics of Propulsion*, Vol. 1, Addison-Wesley, Reading, MA, 1992, p. 764.
- [36] Liu, X., Sun, D., and Sun, X., "Basic Studies of Flow-Instability Inception in Axial Compressors Using Eigenvalue Method," *Journal of Fluids Engineering*, Vol. 136, No. 3, 2014, Paper 031102.
doi:10.1115/1.4026417
- [37] Peyret, R., *Spectral Methods for Incompressible Viscous Flow*, Springer, New York, 2002, pp. 157–166.
doi:10.1007/978-1-4757-6557-1
- [38] Kovásznay, L. S., "Turbulence in Supersonic Flow," *Journal of the Aeronautical Sciences*, Vol. 20, No. 10, 2012, pp. 657–674.

- [39] Chu, B.-T., and Kovásznay, L. S., "Non-Linear Interactions in a Viscous Heat-Conducting Compressible Gas," *Journal of Fluid Mechanics*, Vol. 3, No. 5, 1958, pp. 494–514.
doi:10.1017/S0022112058000148
- [40] Stow, S., Dowling, A., and Hynes, T., "Reflection of Circumferential Modes in a Choked Nozzle," *Journal of Fluid Mechanics*, Vol. 467, Sept. 2002, pp. 215–239.
doi:10.1017/S0022112002001428
- [41] Rusak, Z., and Morris, W. J., "Stall Onset on Airfoils at Moderately High Reynolds Number Flows," *Journal of Fluids Engineering*, Vol. 133, No. 11, 2011, Paper 111104.
doi:10.1115/1.4005101
- [42] Rusak, Z., "Subsonic Flow Around the Leading Edge of a Thin Aerofoil with a Parabolic Nose," *European Journal of Applied Mathematics*, Vol. 5, No. 3, 1994, pp. 283–311.
doi:10.1017/S0956792500001479
- [43] Woodley, B., and Peake, N., "Resonant Acoustic Frequencies of a Tandem Cascade. Part 1. Zero Relative Motion," *Journal of Fluid Mechanics*, Vol. 393, Aug. 1999, pp. 215–240.
doi:10.1017/S0022112099005601
- [44] Cooper, A., Parry, A., and Peake, N., "Acoustic Resonance in Aeroengine Intake Ducts," *Journal of Turbomachinery*, Vol. 126, No. 3, 2004, pp. 432–441.
doi:10.1115/1.1776586
- [45] Hathaway, M., Chriss, R., Strazisar, A., and Wood, J., "Laser Anemometer Measurements of the Three-Dimensional Rotor Flow Field in the NASA Low-Speed Centrifugal Compressor," NASA Lewis Research Center TP-3527, 1995.
- [46] Frigne, P., and Van den Braembussche, R., "Distinction Between Different Types of Impeller and Diffuser Rotating Stall in a Centrifugal Compressor with Vaneless Diffuser," *Journal of Engineering for Gas Turbines and Power*, Vol. 106, No. 2, 1984, pp. 468–474.
doi:10.1115/1.3239589

M. N. Glauser
Associate Editor